

A Computational Fluid Dynamics study of drug-releasing ocular implants for glaucoma treatment: Comparison of implant size and locations

Elisa Molla¹, Tao Chen¹, Cynthia Yu-Wai-Man², Daniel Sebastia-Saez¹

¹School of Chemistry and Chemical Engineering, University of Surrey, Guildford, GU2 7XH, UK

²Faculty of Life Sciences & Medicine, King's College London, London, SE1 1UL, UK

Keywords

Computational Fluid Dynamics; Glaucoma; Intraocular pressure; drug-releasing implant; drug delivery

Corresponding Authors:

Cynthia Yu-Wai-Man, King's College London, cynthia.yu-wai-man@kcl.ac.uk

Daniel Sebastia-Saez, University of Surrey, j.sebastiasaez@surrey.ac.uk

List of symbols

Latin symbols

c – Concentration; $\text{mol}\cdot\text{m}^{-3}$

D – Diffusion coefficient; $\text{m}^2\cdot\text{s}^{-1}$

\vec{g} – Acceleration due to gravity; $\text{m}\cdot\text{s}^{-2}$

h_C, h_i, h_{il} – Height of anterior chamber, iris and iris-lens channel respectively; mm

I – Identity matrix

\vec{J} – Molar flux; $\text{mol}\cdot\text{m}^{-2}\cdot\text{s}^{-1}$

k_b – Boltzmann constant; $\text{J}\cdot\text{K}^{-1}$

L_{TM} – Length of the trabecular meshwork; mm

MW – Molecular weight; Da

p – Pressure; Pa

r – Molecular radius; Å

R_C, R_L, R_p – Radius of posterior cornea, lens and pupil respectively; mm

T – Temperature; K

\vec{u} – Velocity; $\text{m}\cdot\text{s}^{-1}$

Greek symbols

μ – Dynamic viscosity; $\text{Pa}\cdot\text{s}$

ρ – Density; $\text{kg}\cdot\text{m}^{-3}$

Other symbols

∇ – Nabla operator

Abstract

Drug-releasing implants are gaining momentum in the treatment of glaucoma. Implants present however several limitations. Among these limitations, there is the inability to provide an even distribution of the drug in the trabecular meshwork. CFD simulations were used in this work to study the interplay between ocular fluid dynamics and drug diffusion to explore the options to achieve a homogeneous drug distribution. The analysis finds that the balance between convection and diffusion flux hinders mixing within the eye's anterior chamber. This results in highly localised drug delivery in the trabecular meshwork when using a gravity-driven location implant. The results also show that varying the size of the implant can help to solve the issue. Given the natural variability of the trabecular meshwork size amongst patients, implants with personalised size may become a potential solution. The location of the implant within the eye is also key to effective drug delivery. Natural laminar flow of aqueous humour within the eye's anterior chamber prevents achieving an even drug distribution at the target tissue for gravity-driven location implants. However, the iris-lens gap can be utilised as a natural mixer when placing the implant in the eye's posterior chamber, thus helping with effective delivery.

1. Introduction

Glaucoma is a chronic, progressive optic neuropathy affecting around 70 million people worldwide¹. This condition is characterised by elevated intraocular pressure (IOP), which results from increased resistance to the outflow of aqueous humour (AH). Glaucoma causes irreversible damage to the optic nerve and ultimately, blindness². Figure 1 shows a schematic of the anterior chamber and the conventional outflow pathway of the AH. It is produced at the ciliary body at a rate between $1.5 \mu\text{l}/\text{min}$ and $3 \mu\text{l}/\text{min}$ ³. From there, the fluid flows through the

posterior portion of the iris into the anterior chamber (AC) of the eye. It then reaches the trabecular meshwork (TM), where it is absorbed into the systemic circulation through the collector channels of the Schlemm's canal. That conventional outflow pathway is responsible for the evacuation of between 80 and 90% of the AH, with the alternative route being the uveoscleral pathway^{4,5}, where the AH diffuses through the intercellular spaces of the ciliary body and is responsible for the evacuation of the remaining AH. The uveoscleral pathway has not been considered in this study.

Glaucomatous conditions can develop in two ways, including open-angle glaucoma and closed-angle glaucoma. In open-angle glaucoma, the most common type of glaucoma, the TM loses its capacity to evacuate the AH due to fibrosis. The TM consists of an extracellular matrix (ECM), which is formed of collagen, fibronectin, fibrillin and hyaluronic acid and is filled with trabecular cells. Fibrosis, which is the excessive deposition of the ECM components in the TM leads to a reduced evacuation capability of the AH, hence resulting in increased IOP⁶. Under normal physiological conditions, IOP ranges between 10–21 mmHg. The risk of developing glaucoma increases significantly with IOP readings exceeding 21 mmHg. Closed-angle glaucoma is less common than open-angle glaucoma, and is characterised by an abnormally narrow iridocorneal angle, which results in increased resistance of AH outflow. The simulations included in this study reproduce an open-angle glaucoma scenario.

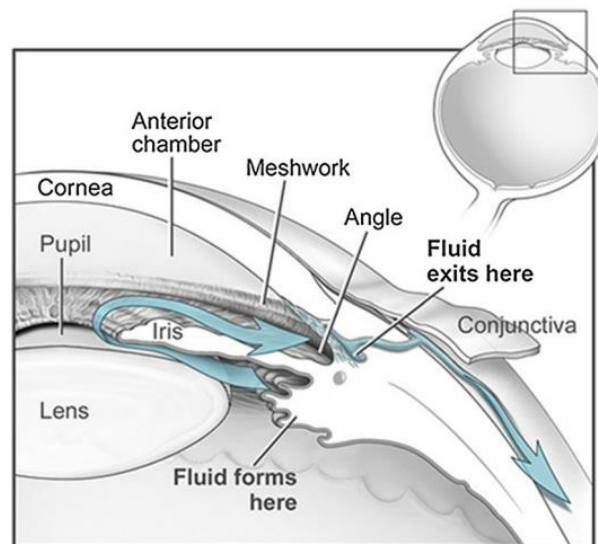


Figure 1 Schematic illustration of aqueous humour flow within the eye's anterior chamber. Image reproduced with permission from ⁷

The most common way to treat glaucoma focus on regulating IOP using topical eye drops that either reduce AH production (e.g., beta blockers) and/or outflow resistance⁸. Another common

option is laser trabeculoplasty, which includes Selective Laser Trabeculoplasty (SLT) and Argon Laser Trabeculoplasty (ALT). These methods target the tissue of the TM to facilitate drainage. Invasive surgical interventions, like trabeculectomy and tube surgery, may become necessary in severe cases, but can cause side effects, such as cataract formation, hypotony and endophthalmitis⁹. In the case of closed-angle glaucoma, several forms of surgery exist, including laser iridotomy and iridoplasty.

The effectiveness of treatments based on eye drops relies heavily on patients' adherence, which is generally poor¹⁰. Extensive efforts have been put into improving patient adherence, including motivational patient interviewing by glaucoma educators, colour coding bottle caps, self-reporting, real-time electronic monitoring systems and prescription refill rate monitoring. Negative attitude towards these types of treatments is the main cause of non-adherence. Hence, it is concluded that the optimal treatment option would provide a sustained drug release over time with zero reliance on patient adherence. Given the limitations of topical treatments and surgery, the use of drug reservoirs, such as punctal plugs and external ocular inserts, is gaining momentum of late^{11,12}.

To date, Durysta[®] is the only implant approved by the FDA and available commercially^{13,14}. Durysta[®] is placed in the lower part of the iridocorneal angle, at the entry to the TM. With its standard cylindrical dimensions (i.e. diameter 0.2 mm and 1 mm length), one of the concerns with the use of Durysta[®] is the difficulty to achieve a homogeneous concentration of the released drug across the TM. This work is concerned with how to solve this problem. While the placement of Durysta[®] in the AC is driven by gravity, there are other placement solutions being developed. For instance, the travoprost implant iDose[®] TR uses a trabecular anchor^{15,16}. Further, another method under clinical trial at present is based on attaching a ring-shaped drug reservoir on the haptic legs of intraocular lenses (IOL) used in cataract surgery (<https://www.spyglasspharma.com>)

Understanding the interplay between ocular fluid dynamics and mass transport is key to accelerate the development of effective IOP-reducing drug-releasing ocular implants. Mathematical simulations (i.e., *in-silico* methods) are gaining momentum as some authors highlight the small size of the AC and the implant as a limitation to carry out their experimental studies¹⁷, among other difficulties, including ethical issues. Further, *in-silico* methods can contribute to test different implant-location and size scenarios in a swift manner, hence suggesting further ways of drug delivery improvement.

There is a growing number of studies that deal with simulations of drug diffusion within the eye using Computational Fluid Dynamics (CFD). The flow of the aqueous humour has been extensively validated in many studies. An example of the aqueous humour flow description can be seen in¹⁸, where the authors simulate the flow of AH in the collector channels of the Schlemm's canal. Another example was reported in¹⁹, where CFD was used to simulate both a healthy and a glaucomatous IOP condition. An example of drug diffusion simulation is the work reported in²⁰, where administration of timolol using therapeutic contact lenses was simulated. Recent work describes a detailed simulation of a drug-releasing, ring-shaped implant mounted on the haptic legs of an IOL³¹. The authors simulate how the release of the drug reduces the resistance to the AH flow in the TM, which is described as a porous medium using Darcy's law.

In this work, we used CFD simulations to test three methods to achieve a homogeneous drug distribution in the trabecular meshwork. The first hypothesis is concerned with the balance between convection and diffusion encountered during the operating time of the implant. Convection-dominated flow would give rise to narrowly localised drug delivery in part of the TM when the implant is placed in its vicinity, while if diffusion dominates then the drug could be evenly distributed. The research question is thus whether diffusion can dominate over convection by reducing the molecular size of the drug. The second hypothesis proposes varying the size of the implant to obtain an even drug distribution on the target tissue. In such case, localised delivery could be countered by choosing an appropriate diameter of the implant, close to the size of the TM. The third hypothesis is concerned with improving mixing in laminar flows. Placing the implant between the iris and the lens would result in the iris having a mixing effect similar way to how baffles are used in static mixers²¹. The hydrodynamics of ocular drug-releasing implants placed in the iridocorneal angle and on the haptic legs of an IOL are thus compared to decide which implant placement gives rise to the best treatment efficacy.

2. Methodology

Calculations were performed using the commercial FEM software COMSOL Multiphysics v6.1. A 2-D axisymmetric section of the eye geometry was implemented (geometry parameters included in Table 1 and schematic in Figure 2). The 2-D description is enough to obtain the qualitative descriptions of the drug's concentration profiles at the TM and test the hypotheses of this study. An accurate description of the hydrodynamic effects at both ends of the implant is not required to test these hypotheses, hence the choice for a 2-D geometry over a 3-D

approach, although the cylindrical shape of Durysta[®] breaks the axial symmetry. Further, the axisymmetric 2-D geometry used here represents accurately the geometry of the ring-shaped implant tested clinically by SpyGlass PharmaTM. The concentration profile of the drug at the entry to the TM is used as a proxy to signal the drug's bioavailability and homogeneous distribution within the porous TM tissue.

A no-slip boundary condition was implemented in the cornea, lens, iris, and haptic legs of the implant. A normal inflow velocity ($v_0 = 2.03 \mu\text{m}\cdot\text{s}^{-1}$) was established on the AH inlet (0.5 mm thickness), which corresponds to an AM production flow rate of $2.5 \mu\text{l}\cdot\text{min}^{-1}$, similarly to the parameters implemented in²². An outlet was set on the TM. Both the AH inlet and the TM are highlighted in red in Figure 2. The position of the eye's symmetry axis is also shown. The static pressure within the AC was set at 27 mmHg to simulate a glaucomatous state⁷. Figure 2 displays the x-axis origin and direction of reckoning of the concentration profiles included in the results section of this work. The zero corresponds to the top part of the TM. The schematic also shows the gravity-driven position of the Durysta[®] implant and the position of the implant on the haptic legs of the IOL. It can be seen that the Durysta[®] implant does not shadow the entirety of the outlet, which has consequences on the homogeneity of the concentration profiles along the entrance to the TM.

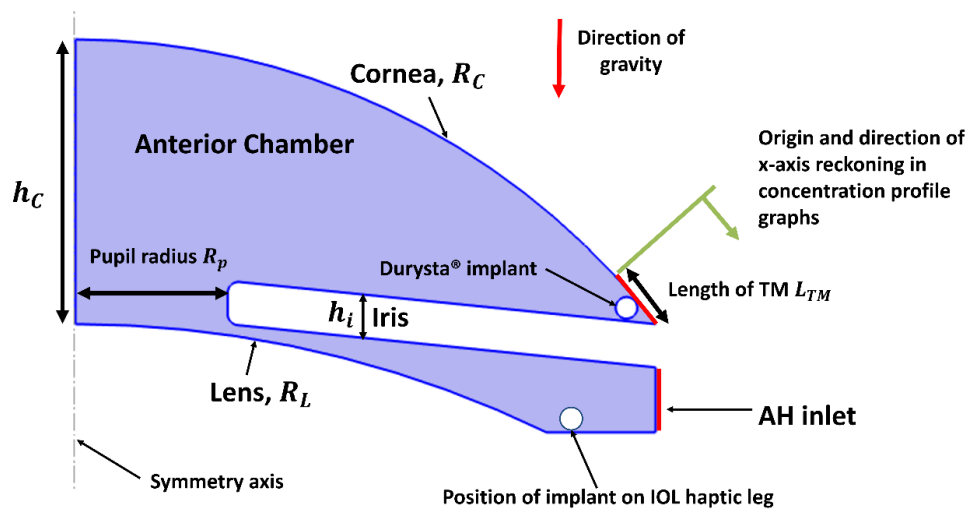


Figure 2. Schematic illustration of the geometric reconstruction of the 2-D axisymmetric section of the eye's geometry in COMSOL Multiphysics v6.1. The schematic includes the standard gravity-driven location of the Durysta[®] implant in the iridocorneal angle, and the location tested on the IOL haptic legs. The schematic shows the direction of the x-axis reckoning for the concentration profiles included in the results section.

Table 1 Geometry parameters of the human eye used in the 2-D axisymmetric geometry of the eye.

Parameter	Value [mm]
Radius of posterior cornea R_C ⁷	6.80
Maximum height of anterior chamber h_C ⁷	2.63
Lens radius R_L ⁷	10.00
Height of iris-lens channel h_{il} ^{7,23,24}	0.093
Iris thickness h_i ²⁵	0.40
Pupil radius R_p ^{24,26}	1.75
Length of TM L_{TM} ^{27,28}	0.73

A stationary study using an infinite dose was chosen since Durysta[®] releases bimatoprost over the course of several months, creating a prolonged steady state condition within the eye. Durysta[®] implements a dose of 10 mcg of bimatoprost. The implant has a cylindric shape with 0.2 mm of diameter and 1 mm height. This yields an initial concentration of 768 mol·m⁻³. The model is single-phase and solves the mass and momentum conservation equations:

$$\rho \nabla \cdot \vec{u} = 0 \quad (1)$$

$$\rho(\vec{u} \cdot \nabla)\vec{u} = \nabla \cdot [-pI + \mu(\nabla\vec{u} + (\nabla\vec{u})^T)] + \rho\vec{g} \quad (2)$$

Where ρ represents the density, \vec{u} is the velocity vector, μ is the dynamic viscosity of water, p is the pressure, I is the identity matrix, and \vec{g} is the acceleration due to gravity. Differences can be seen in the literature regarding the velocity field in the AC depending on the direction of gravity, with differences of up to 12% in the maximum velocity in the iris-lens gap^{7,29}. A study also linked the eye position to changes in IOP³⁰. The eye was considered in supine position in this study to minimise the effect of gravity on the bulk movement of AH towards the TM.

The mass and momentum equations were coupled with the steady-state transport equation:

$$\nabla \cdot \vec{j} + \vec{u} \cdot \nabla c = 0 \quad (3)$$

Where c is the concentration of the drug and $\vec{j} = -D\nabla c$ accounts for Fick's diffusion flux. The diffusion coefficient in water was calculated using the well-known Stokes-Einstein equation:

$$D = \frac{k_b T}{6\pi\mu r} \quad (4)$$

Where $T = 34.51^\circ\text{C}$ is the temperature of the eye and $\mu = 0.7269 \text{ mPa}\cdot\text{s}$ is the dynamic viscosity of water at that temperature. The parameter $k_b = 1.380649 \times 10^{-23} \text{ J/K}$ is the Boltzmann constant. The molecular radius r was calculated using the empirical expression:

$$r = \sqrt[3]{\frac{3}{4\pi} \times 0.9087 \times MW} \quad (5)$$

Which assumes spherical symmetry.

3. Results and discussion

3.1. Hypothesis #1: Convection/diffusion balance in drug-releasing intraocular implants hinders homogeneous delivery in the TM.

Velocity at inlet boundary ($v_0 = 2.03 \mu\text{m}\cdot\text{s}^{-1}$) was adjusted to an AH input flow rate of $2.5 \mu\text{l}\cdot\text{min}^{-1}$. This gave as a result the velocity contour plot included in Figure 3. The maximum velocity observed in the iris-lens channel was $61 \mu\text{m}\cdot\text{s}^{-1}$. Some authors observe a maximum velocity in the iris-lens gap around $900\text{--}1000 \mu\text{m/s}^{7,23,29}$. An additional set of simulations has been carried out with a normal inflow velocity of $30 \mu\text{m}\cdot\text{s}^{-1}$ (input flow rate of $31.31 \mu\text{l}\cdot\text{min}^{-1}$), which gave way to a maximum velocity of $930 \mu\text{m/s}$ in the iris-lens gap, hence close to *in-silico* observations in the literature. These simulations gave rise to results where the effect of convection over diffusion was accentuated. These differences are attributed to variations in the parameters defining the geometry of the eye, specifically the iris-lens gap. The plot includes the geometry of the Durysta[®] implant in the iridocorneal angle. The simulation also shows convective acceleration of the AH in the vicinity of the implant due to the partial blocking of the flow entering the TM.

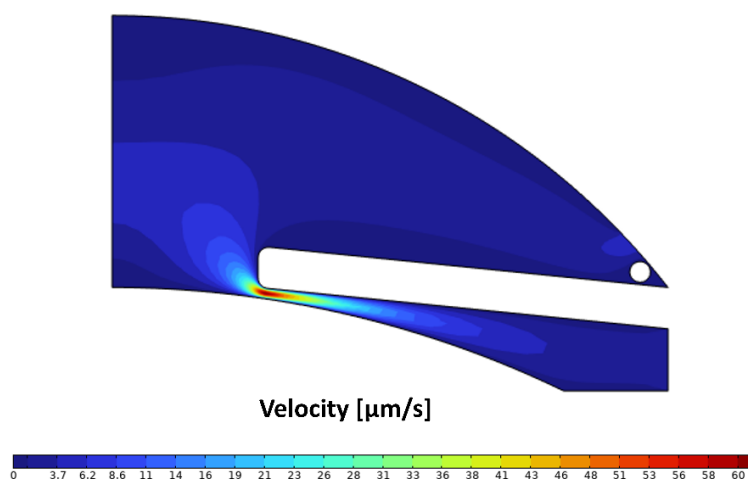


Figure 3 Velocity contour plot of aqueous humour within the anterior chamber.

A grid independence check was performed over the value of the aqueous humour velocity in a probe point on the iris-lens channel at steady-state using all nine mesh density degrees (i.e., from *Extremely Coarse* to *Extremely Fine*) available in COMSOL Multiphysics for the *Physics Controlled Mesh* option. The difference between the two densest mesh options was $< 0.2\%$. The *Extremely Fine* mesh option (25,115 elements) was used to obtain the rest of the results in this work due to the small computational time of the model.

Table 2 A list of compounds used for drug-releasing glaucoma implants (National Eye Institute \rightarrow glaucoma medicines).

Group	Compound	MW [Da]	D [$\mu\text{m}^2/\text{s}$]
Prostaglandins	Latanoprost	432	685
	Travoprost	500	652
	Tafluprost	452	674
	Bimatoprost	415	694
Rho kinase inhibitor	Netarsudil	453	674
Nitric Oxides	Latanoprostene Bunod	507	649
Miotic or cholinergic agents	Pilocarpine	208	874

Table 2 shows the molecular weight and the diffusion coefficients of common drugs for the treatment of glaucoma by helping fluid drain through the TM (<https://www.nei.nih.gov/Glaucoma/glaucoma-medicines>). The table shows that the drugs are within a MW range between 200–500 Da, which implies diffusion coefficients within the range 885–652 $\mu\text{m}^2/\text{s}$. Contour concentration profiles were obtained mimicking the Durysta[®] implant

by using an infinite dose ($c_0 = 768 \text{ mol/m}^3$) for the compounds with the greatest and smallest MW among those included in Table 2 (i.e., pilocarpine and latanoprostene bunod). The concentration profiles of any other compounds included in Table 2 would lie between the two shown in Figure 4, including the compound in the Durysta[®] implant, bimatoprost. The concentration profiles show that the magnitude of convection and diffusion flux gives way to similar concentration profiles, with the portion of the TM shadowed by the implant reaching maximum concentration $c = 768 \text{ mol/m}^3$ (i.e., Distance along TM $> 0.37 \text{ mm}$). The concentration that reaches the upper part of the TM (i.e., Distance along TM $< 0.37 \text{ mm}$) is less than half the infinite dose in the implant. It would be necessary to decrease the diffusion coefficient below practical limits to obtain an evenly distributed concentration along the TM. It can be concluded that using an implant with a small enough MW is not a valid strategy to obtain an even distribution of the drug entering the TM.

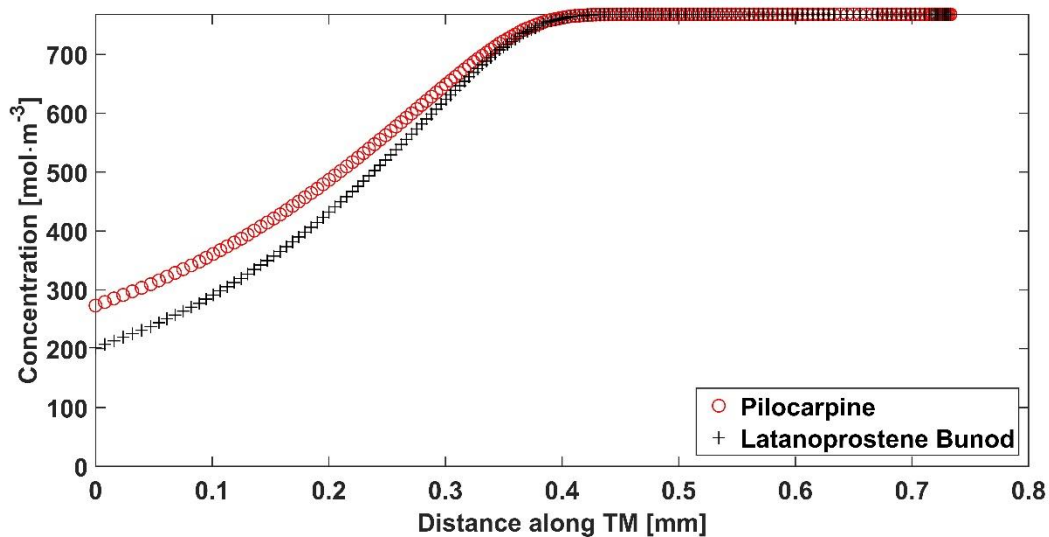


Figure 4 Concentration profiles along the TM for pilocarpine and latanoprostene bunod. The zero in the x-axis corresponds to the top part of the TM, as shown in the schematic in Figure 2.

3.2. Hypothesis #2: Personalised implant size can help with homogeneous delivery in the TM

Figure 5 shows the effect of the implant size on the concentration profiles along the TM for the base case of bimatoprost delivery using Durysta[®] ($r = 0.1 \text{ mm}$) and a hypothetical implant with a radius $r = 0.3 \text{ mm}$. The latter shadows the entirety of the TM. The production rate of AH and the drug dosage have been maintained to isolate the effect of implant size. It can be seen that using the Durysta[®] standard measures results in differences in concentration between the upper and the lower part of the TM. This can be attributed to Durysta[®] not shadowing the entirety of

the TM combined with the laminar characteristics of the flow of AH and the importance of diffusion flux relative to convection flux. Tripling the radius gives rise to a homogeneous concentration profile. The model suggests thus that, due to the laminar characteristics of the AH flow, adapting the diameter of the implant to the size of the TM of the patient can give rise to improved drug delivery.

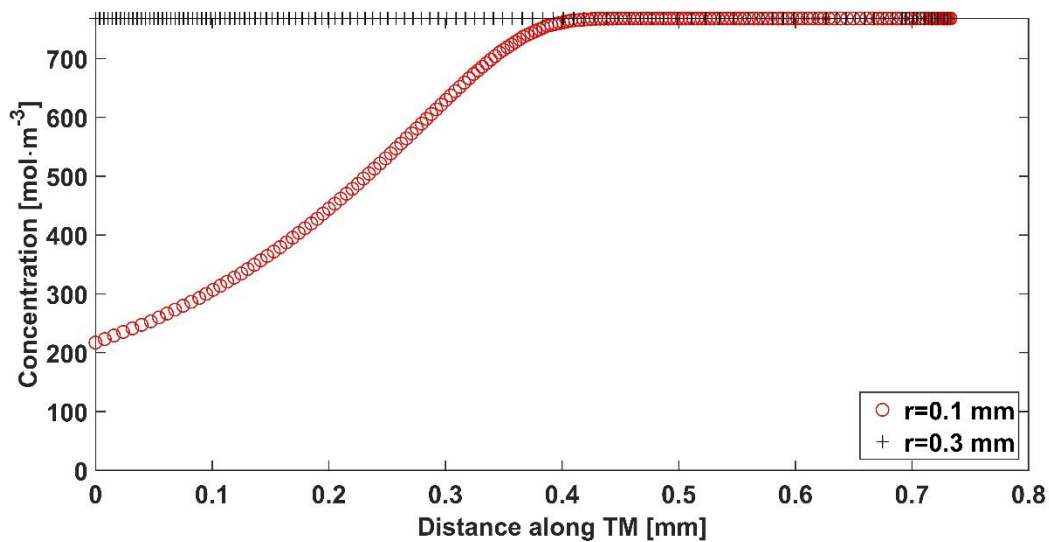


Figure 5 Concentration profiles along the TM for bimatoprost. The red data series correspond to the radius of Durysta[®] ($r=0.1$ mm). The black data series corresponds to a hypothetical implant with the same compound (i.e., bimatoprost) and concentration as Durysta[®] but tripling the radius to shadow the entirety of the TM. The zero in the x-axis corresponds to the top part of the TM, as shown in the schematic in Figure 2.

3.3. Hypothesis #3: The iris can be used as a natural mixer to improve homogeneous delivery

Another possibility to attain homogeneous drug concentrations in the TM is to change the placement of the implant. The results in Figure 6 show the comparison between the concentration profile of bimatoprost using the base-case of the gravity-driven placement of Durysta[®] as shown in the previous Figure 5 and an analogous reservoir placed in the haptic legs of an IOL before the iris-lens gap. The latter gives rise to a constant concentration along the TM, although smaller in value than that obtained with the standard location of Durysta[®] at the iridocorneal angle.

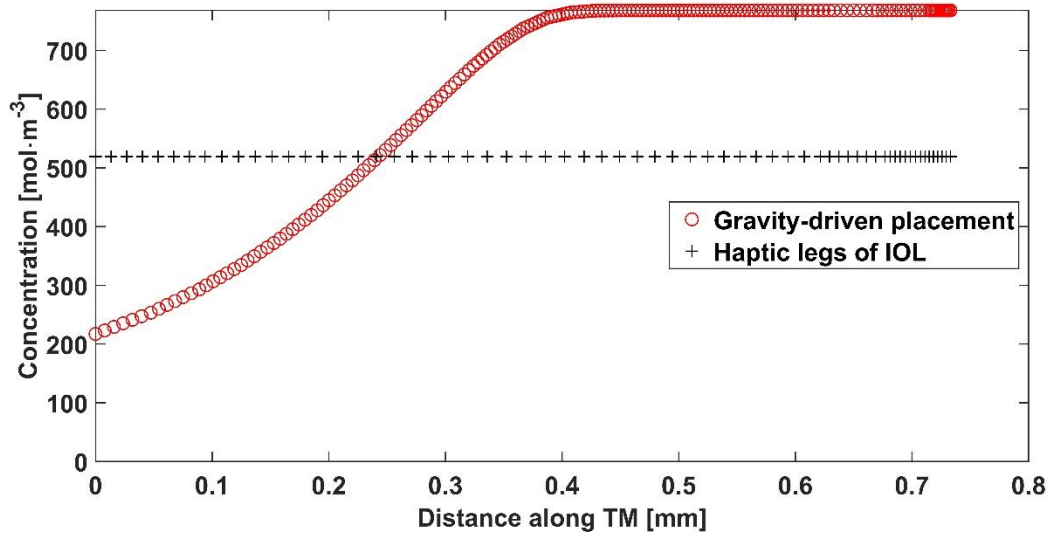


Figure 6 Concentration profiles along the TM for bimatoprost. The red data series corresponds to the standard gravity-driven placement of Durysta® at the iridocorneal angle. The black data series corresponds to the hypothetical placement of the same implant in the haptic legs of the IOL. The zero in the x-axis corresponds to the top part of the TM, as shown in the schematic in Figure 2

4. Conclusions

An *in-silico* model of drug-releasing implants in the anterior chamber of the eye is presented in this work. Our results suggest that there is a precise balance between convection and diffusion that results in drug release being highly localised on a small portion of the TM when the implant is placed at the iridocorneal angle.

The model also suggests that an increase in the diffusion flux relative to convection using the smallest compound available in terms of molecular weight is not enough to attain homogeneous drug concentrations in the trabecular meshwork. This leaves the modification of the implant's geometry and its location as the sole options to deliver a homogeneous concentration distribution over the TM.

In terms of implant size, results of the concentration profiles were obtained for two sizes of the implant at the iridocorneal angle. Our results suggest that the diameter of the implant must be similar to the size of the patient's TM to attain a homogeneous drug concentration at the TM. The natural variability in the size of the TM hints the importance of personalised implants.

Regarding the location of the implant within the eye, our results suggest that placing the implant before the iris-lens gap (i.e., in the flow direction of the AH) gives rise to homogeneous concentrations in the TM, although smaller than in the case of placing the implant at the iridocorneal angle. This is due to the laminar character of the aqueous humour flow within the anterior chamber, which hinders mixing. Placing the implant next to the ciliary body results in

the use of the iris-lens gap as a natural mixer, which results in the homogeneous drug concentrations observed in the trabecular meshwork.

Funding

This work is supported by the Medical Research Council (grant number MR/T027932/1).

REFERENCES

1. Faiq, M. A. *et al.* A novel mathematical model of glaucoma pathogenesis. *J Curr Glaucoma Pract* **13**, 3–8 (2019).
2. Killer, H. E. & Pircher, A. What is the optimal glaucoma treatment: reducing aqueous humour production or facilitating its outflow? *Eye (Basingstoke)* vol. 34 1719–1721 Preprint at <https://doi.org/10.1038/s41433-020-0862-8> (2020).
3. Goel, M., Picciani, R. G., Lee, R. K. & Bhattacharya, S. K. *Aqueous Humor Dynamics: A Review. The Open Ophthalmology Journal* vol. 4 (2010).
4. Weinreb, R. N., Aung, T. & Medeiros, F. A. The pathophysiology and treatment of glaucoma: A review. *JAMA* vol. 311 1901–1911 Preprint at <https://doi.org/10.1001/jama.2014.3192> (2014).
5. Johnson, M., McLaren, J. W. & Overby, D. R. Unconventional aqueous humor outflow: A review. *Experimental Eye Research* vol. 158 94–111 Preprint at <https://doi.org/10.1016/j.exer.2016.01.017> (2017).
6. Qin, M. & Yu-Wai-Man, C. Glaucoma: Novel antifibrotic therapeutics for the trabecular meshwork. *European Journal of Pharmacology* vol. 954 Preprint at <https://doi.org/10.1016/j.ejphar.2023.175882> (2023).
7. Wang, W., Qian, X., Song, H., Zhang, M. & Liu, Z. Fluid and structure coupling analysis of the interaction between aqueous humor and iris. *Biomed Eng Online* **15**, (2016).
8. Conlon, R., Saheb, H. & Ahmed, I. I. K. Glaucoma treatment trends: a review. *Canadian Journal of Ophthalmology* vol. 52 114–124 Preprint at <https://doi.org/10.1016/j.jcjo.2016.07.013> (2017).
9. Cursiefen, C., Cordeiro, F., Cunha-Vaz, J., Wheeler-Schilling, T. & Scholl, H. P. N. Unmet Needs in Ophthalmology: A European Vision Institute-Consensus Roadmap 2019–2025. *Ophthalmic Research* vol. 62 123–133 Preprint at <https://doi.org/10.1159/000501374> (2019).
10. Walters, T. R., Lee, S. S., Goodkin, M. L., Whitcup, S. M. & Robinson, M. R. Bimatoprost Sustained-Release Implants for Glaucoma Therapy: 6-Month Results From a Phase I/II Clinical Trial. *Am J Ophthalmol* **175**, 137–147 (2017).
11. Kesav, N. P., Capitena Young, C. E., Ertel, M. K., Seibold, L. K. & Kahook, M. Y. Sustained-release drug delivery systems for the treatment of glaucoma. *International Journal of Ophthalmology* vol. 14 148–159 Preprint at <https://doi.org/10.18240/ijo.2021.01.21> (2021).

12. Ozdemir, S., Wong, T. T., Allingham, R. R. & Finkelstein, E. A. Predicted patient demand for a new delivery system for glaucoma medicine. *Medicine (United States)* **96**, (2017).
13. Bacharach, J. *et al.* Phase 3, Randomized, 20-Month Study of the Efficacy and Safety of Bimatoprost Implant in Patients with Open-Angle Glaucoma and Ocular Hypertension (ARTEMIS 2). *Drugs* **81**, 2017–2033 (2021).
14. Medeiros, F. A. *et al.* Phase 3, Randomized, 20-Month Study of Bimatoprost Implant in Open-Angle Glaucoma and Ocular Hypertension (ARTEMIS 1). *Ophthalmology* **127**, 1627–1641 (2020).
15. Sarkisian, S. R. *et al.* Travoprost Intracameral Implant for Open-Angle Glaucoma or Ocular Hypertension: 12-Month Results of a Randomized, Double-Masked Trial. *Ophthalmol Ther* **13**, 995–1014 (2024).
16. Bacharach, J. *et al.* Travoprost Intracameral Implant Demonstrates Superior IOP Lowering Versus Topical Prostaglandin Analog Monotherapy in Patients with Open-Angle Glaucoma or Ocular Hypertension. *Ophthalmol Ther* (2024) doi:10.1007/s40123-024-00992-1.
17. Weinreb, R. N. *et al.* Single Administration of Bimatoprost Implant: Effects on 24-Hour Intraocular Pressure and 1-Year Outcomes. *Ophthalmol Glaucoma* **6**, 599–608 (2023).
18. Martínez Sánchez, G. J., Escobar del Pozo, C., Rocha Medina, J. A., Naude, J. & Brambila Solorzano, A. Numerical simulation of the aqueous humor flow in the eye drainage system; a healthy and pathological condition comparison. *Med Eng Phys* **83**, 82–92 (2020).
19. Martínez Sánchez, G. J., Escobar del Pozo, C., Rocha Medina, J. A., Naude, J. & Brambila Solorzano, A. Numerical simulation of the aqueous humor flow in the eye drainage system; a healthy and pathological condition comparison. *Med Eng Phys* **83**, 82–92 (2020).
20. Yi, H., Feng, Y. & Gappa-Fahlenkamp, H. Analysis of topical dosing and administration effects on ocular drug delivery in a human eyeball model using computational fluid dynamics. *Comput Biol Med* **141**, (2022).
21. Bennour, E. *et al.* Improving mixing efficiency in laminar-flow static mixers with baffle inserts and vortex generators: A three-dimensional numerical investigation using corrugated tubes. *Chemical Engineering and Processing - Process Intensification* **193**, (2023).
22. Cai, J. C., Chen, Y. L., Cao, Y. H., Babenko, A. & Chen, X. Numerical study of aqueous humor flow and iris deformation with pupillary block and the efficacy of laser peripheral iridotomy. *Clinical Biomechanics* **92**, (2022).
23. Ferreira, J. A., De Oliveira, P., Da Silva, P. M. & Murta, J. N. Numerical simulation of aqueous humor flow: From healthy to pathologic situations. *Appl Math Comput* **226**, 777–792 (2014).
24. Fernández-Vigo, J. I. *et al.* Computational simulation of aqueous humour dynamics in the presence of a posterior-chamber versus iris-fixed phakic intraocular lens. *PLoS One* **13**, (2018).

25. Cui, L. *et al.* Study on the correlation between iris blood flow, iris thickness and pupil diameter in the resting state and after pharmacological mydriasis in patients with diabetes mellitus. *BMC Ophthalmol* **24**, (2024).
26. Spector, R. H. *58 The Pupils*.
27. Basson, N. *et al.* A computational fluid dynamics investigation of endothelial cell damage from glaucoma drainage devices. *Sci Rep* **14**, (2024).
28. Kumar, S., Acharya, S., Beuerman, R. & Palkama, A. Numerical solution of ocular fluid dynamics in a rabbit eye: Parametric effects. *Ann Biomed Eng* **34**, 530–544 (2006).
29. Villamarin, A. *et al.* 3D simulation of the aqueous flow in the human eye. *Med Eng Phys* **34**, 1462–1470 (2012).
30. Petersen, L. G. *et al.* Gravitational effects on intraocular pressure and ocular perfusion pressure. *J Appl Physiol* **132**, 24–35 (2022).
31. Pandey, P. K. *et al.* Drug delivery from a rig implant attached to intraocular lens: An in-silico investigation. *J Pharm Sci* In-press. Corrected proof.